Int. J. Nonlinear Anal. Appl. 17 (2026) 5, 43–50
ISSN: 2008-6822 (electronic)
http://dx.doi.org/10.22075/ijnaa.2024.32985.4908

Effects of defects on axial fatigue strength of steel samples and supports produced by additive manufacturing

Ali Nadaf Fard, Abdul Reza Rasti Talab*

Department of Mechanics, Dariun Branch, Islamic Azad University, Dariun, Iran

(Communicated by Seyed Hossein Siadati)

Abstract

Many materials such as steel, aluminium and titanium alloys can be realised by powder bed solutions, melting subsequently powder layers utilizing laser or electron beam (Laser Beam Melting LBM and Electron Beam Melting EBM). The microstructure is realised by layer-by-layer solidification. Having a high cooling rate cannot be considered isotropic. Therefore, the mechanical properties could be influenced by the building direction. Regarding maraging steel, the study of the influence of the building direction and the heat treatment on the static and axial fatigue strength has been investigated in a previous contribution. A large scatter of the fatigue test results was found because of the presence of detrimental and subsurface defects. This contribution aims to present additional axial fatigue-test results of maraging steel characterized by different build orientations and provide an analysis of the defects observed at the crack initiation area of the fracture surface.

Keywords: Effects, defects, fatigue, strength, supports
2020 MSC: 70K30, 37N20

1 Introduction

In PBF technologies like Selective Laser Melting (SLM) or Direct Metal Laser Sintering (DMLS), as well as Electron Beam Melting (EBM), layers of metal powder are melted sequentially by a laser or an electron beam source. This process aims to produce the part designed by CAD software without the typical constraints associated with traditional manufacturing processes [1]. With optimised AM process parameters, the occurrence of defects is almost unavoidable, and it can lead to failure for AM-manufactured parts, especially in applications subject to cyclic loads and fatigue. The primary benefit of embracing an additive manufacturing (AM) process is the ability to manufacture components with customized and intricate geometries. In terms of structural considerations, topological optimization becomes a crucial aspect in the design for additive manufacturing, aiming to maximize the performance of the component under a specified set of loading conditions.

According to the literature, the implementation of design for additive manufacturing (AM) is currently limited to the aerospace, aeronautical, and automotive sectors. This restriction is attributed to the fact that the current advantages of this emerging manufacturing process lie in the production. of customized components with low production volumes. primarily due to the elevated costs associated with the process.

*Corresponding author
Email addresses: a.nadaf@yahoo.com (Ali Nadaf Fard), ab.rastitalab@iau.ac.ir (Abdul Reza Rasti Talab)

Received: January 2024 *Accepted:* April 2024

In the present day, the Selective Laser Melting (SLM) process has undergone significant development, enabling the production of numerous alloys with static mechanical properties comparable to wrought ones. This progress is substantiated by various contributions in the field [3].

On the flip side, a crucial aspect in the design of additive manufacturing (AM) mechanical parts is the existence of defects, which can degrade the fatigue strength of the material, as indicated by references [7, 8]. The primary factors contributing to lower fatigue performance in AM parts include surface finishing, post-heat treatment, and the unavoidable presence of defects arising from the manufacturing processes [2, 5, 9].

The concept of performance is one of the old concepts, which still has not established any consensus about its nature among experts. According to, performance is synonymous with behavior, and only behaviors that are under the control of the individual should be evaluated as performance. According to performance should be defined as work results. The definition includes a more comprehensive view in which performance means both behavior and results, managing steel produced by Selective Laser Melting (SLM), as documented in reference [6]. The focus is on quantifying the square root of the area of defects located in the crack initiation zone of the fracture surface of the specimens, utilizing a Scanning Electron Microscope (SEM).

2 Materials and methods

2.1 Material and specimen's geometry

In this regard, in the first part of the research (qualitative stage), the thematic analysis strategy was used by the Brown and Clark method to design the research model, and in the second part (quantitative stage), the model obtained from the first part was used using the strategy A survey with structural equation modelling approach was tested and evaluated and validated. As one of the most common forms of qualitative research analysis, thematic or theme analysis is a way to see the text, proper understanding of seemingly unrelated information; analysis of qualitative information; systematic observation of a person or interaction group, situation, organization or culture; and converting qualitative data into quantitative data.

From a design perspective, achieving an accurate estimation of the fatigue limit, defined as the maximum stress ensuring a fatigue life for a specified number of cycles, is not possible without considering the mechanics associated with defects. A key research question is how to relate defects to fatigue life. Different approaches have been researched to find the relationship between defects, applied stress and the number of cycles to failure. Common defects observed in Selective Laser Melting (SLM) parts include incomplete fusion holes with irregular 3D shapes, referred to in the literature as Lack Of Fusion (LOF). Additionally, other defects such as pores with elliptical or spherical shapes and crack-like defects can be identified. The mechanisms behind the formation of these defects are explained in the literature. As is well-known from [10], the fatigue strength is controlled by the defects having the maximum size, and given the complex geometries of the LOF is appropriate to adopt the varea parameter. Hence, in certain studies (as noted in [4]), the application of extreme value statistics has been employed to estimate the maximum size of defects based on inspections conducted through CT scanning.

The contribution involves two sets of cylindrical maraging steel specimens. The first batch (E) is manufactured using an EOSINT M280 system, while the second batch is provided by SISMA srl, utilizing the SISMA MYSINT 100 system for the production of components made from maraging steel and other alloys. The material under examination is maraging steel, commonly referred to as 18Ni 300. Table 1 provides the chemical composition of the powders, and Table 2 outlines the process parameters employed in producing the fatigue testing samples.

The geometry of the specimens designed for fatigue testing is illustrated in Fig. 1. For each batch, the specimens were constructed with their axis oriented at both θ° and 90° relative to the building direction, corresponding to the translation of the platform facilitating the deposition of subsequent layers. During the process. The schematic orientation of the samples. is depicted in Fig. 2. Furthermore, half of the total number of specimens underwent ageing heat treatment for 6 hours at a temperature of $490^{\circ}C$ followed by air cooling.

For a clear comprehension of the results in the present contribution, the nomenclature of the single test series is summarized in Table 3, where the prefixes E and S are referred to as EOS and SISMA respectively, 0° and 90° indicate the building direction and NT, T refer to Not heat-Treated and the heat-Treated condition. respectively.

Push-pull constant amplitude fatigue tests were conducted on the Sf batch, and the results were compared with the E batch previously tested, as detailed in reference [6]. Before testing, all specimens underwent a polishing process using progressively finer emery paper, ranging from grade 80 to grade 800. In Fig. 3 deflection of the specimen's axis f, observed in [6].

AD	STA	KN	IN	OC	ITC	AD	LEM	REC	COS	EN	FAF	CA
0.26	0.10	-0.03	0.08	0.10	0.12	0.14	0.13	0.22	0.29	0.23	0.48	0.99
0.29	0.10	0.04	0.05	0.10	0.08	0.14	0.17	0.24	0.28	0.28	0.49	0.99
0.37	0.34	0.50	0.33	0.35	0.23	0.35	0.62	0.47	0.24	0.85	0.91	0.52
0.27	0.34	0.13	0.08	0.33	0.30	0.42	0.36	0.29	0.16	0.28	0.59	0.16
0.40	0.36	0.43	0.42	0.28	0.26	0.35	0.56	0.46	0.18	0.69	0.88	0.40
0.26	0.28	0.45	0.33	0.30	0.20	0.31	0.57	0.36	0.18	0.65	0.86	0.39
0.23	0.09	0.31	0.25	0.11	0.15	0.15	0.37	0.27	0.12	0.58	0.83	0.45
0.36	0.43	0.60	0.44	0.45	0.31	0.40	0.72	0.43	0.18	0.92	0.77	0.17
0.08	0.19	0.37	0.15	0.13	0.02	0.17	0.15	0.12	0.01	0.63	0.39	0.21
0.38	0.38	0.57	0.39	0.39	0.27	0.36	0.67	0.46	0.23	0.94	0.79	0.27
0.27		0.45	0.24	0.21	0.17	0.25	0.44	0.34	0.13	0.89	0.63	0.24
0.29	0.48	0.28	0.27	0.45	0.40	0.46	0.38	0.41	0.98	0.20	0.22	0.27
0.30	0.46	0.21	0.30	0.43	0.41	0.47	0.37	0.42	0.98	0.14	0.19	0.29
0.69	0.58	0.69	0.60	0.57	0.47	0.65	0.88	0.89	0.39	0.60	0.57	0.20
0.68	0.40	0.46	0.46	0.41	0.41	0.61	0.67	0.93	0.39	0.27	0.37	0.26
0.60	0.35	0.34	0.38	0.39	0.38	0.55	0.58	0.88	0.38	0.20	0.30	0.24
0.55	0.60	0.64	0.71	0.55	0.49	0.61	0.63	0.84	0.35	0.33	0.33	0.15
0.48	0.59	0.69	0.51	0.55	0.35	0.57	0.91	0.58	0.30	0.63	0.56	0.05
0.60	0.51	0.51	0.41	0.48	0.43	0.66	0.86	0.70	0.31	0.44	0.55	0.55
0.67	0.61	0.69	0.61	0.60	0.50	0.66	0.93	0.86	0.41	0.59	0.54	0.21
0.34	0.90	0.39	0.48	0.86	0.74	0.87	0.50	0.49	0.50	0.21	0.23	0.12
0.32	0.79	0.38	0.38	0.73	0.57	0.87	0.44	0.47	0.36	0.20	0.19	0.08
0.66	0.53	0.69	0.52	0.45	0.28	0.74	0.73	0.72	0.32	0.48	0.49	0.15
AD	STA	KN	IN	OC	ITC	AD	LEM	REC	COS	EN	FAF	CA

Table 1: Chemical composition of the powder adopted in the batch EOS and SISMA.

Batch	$Fe(WI-\frac{\theta}{a})$	$Ni(WI-)$	$Co(wt-\%)(WI-\frac{\theta}{a})(wt-\%)(Wt-\%)$	$Mo(wt-\%)(WI-\frac{\theta}{a})(wt-\%)(Wt-\%)$	$(wt-\%)(WI-\frac{\theta}{a})(wt-\%)(Wt-\%)$	$Al(wt-\%)(WI-\frac{\theta}{a})(wt-\%)(Wt-\%)$	$Cr(wt-\%)$	$Cu(WI=\frac{\theta}{b})(WI-\frac{\theta}{a})$	$(WI=\frac{\theta}{b})(WI-\frac{\theta}{a})$	$Mn(wt-\%)$	$Si(WI-\frac{b}{a})$	$(WI-\frac{\theta}{n})$	$\lvert(wt-\frac{b}{a})$
EOS	balance	17-19	8.5-9.5	4.5-5.2 0.6-0.8 0.05-	4.5-5.2 0.6-0.8 0.05-	4.5-5.2 0.6-0.8 0.05-	$\leq 0.5\rvert$	≤ 0.5	≤ 0.03	≤ 0.1	≤ 0.1	≤ 0.01	$\lvert \leq 0.0\rvert$
SISMA	balance	17-19	8.5-10	4.5-5.2 0.8-1.2	4.5-5.2 0.8-1.2	/	≤ 0.25	/	≤ 0.03	≤ 0.15	≤ 0.1	≤ 0.01	$\lvert \leq 0.01\rvert$

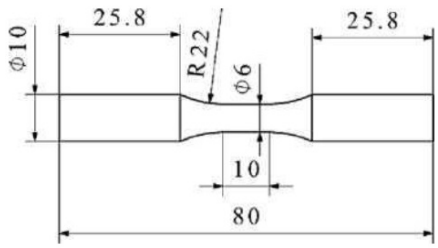

Figure 1: Specimen's geometry

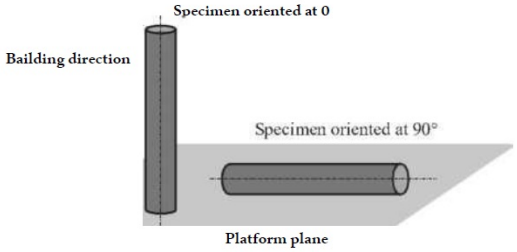

Figure 2: Orientation of specimens axis with respect to the building direction.

Given the understanding that residual stresses induced by the rapid cooling of the melted zone in additive components can lead to geometrical distortion, as demonstrated in reference [6], the gross section of each specimen was turned to mitigate misalignments. Before machining, the deflection of the specimen's axis (denoted as fa in Fig. 3) was measured for all specimens. The fatigue tests were conducted using a servohydraulic SCHENCK HYDROPULS PSA 100 machine equipped with a 100 KN load cell and a TRIO Sistemi RT3 digital controller. The load frequency

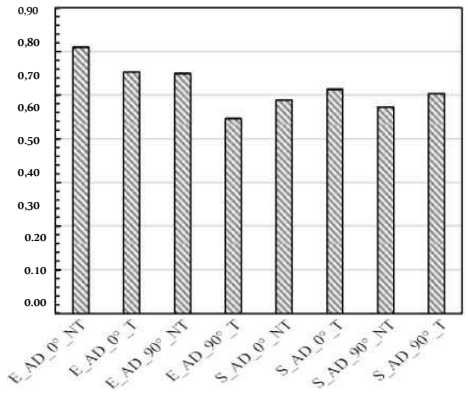

Figure 3: the deflection of the specimen's axis

was adjusted within the range of 10 Hz to 30 Hz, varying based on.

Table 2: Process parameters adopted to manufacture maraging steel specimens for fatigue testing

Batch	Laser power [W]	Laver thickness [pm]	Laser spot diameter [pm]	Laser scan rate	Powder dimension $[pm]$	Temperature of the platform [°C]	Scanning strategy
EOS	400	40	100	Not provided	60	40	Parallel vector
SISMA	120	20	55	500	15-45	Not provided	Not provided

AD	5qrt (AVE)														
	0.83														
ADA	0.53	0,91													
CAC	0.14	0.28	0.99												
CON	0.60	0.35	0.05	0.92											
COS	0.48	0.30	0.29	0.29	0.98										
ENC	0.36	0.34	0.26	0.46	0.18	85									
EXC	0.55	0.31	0.05	0.89	0.26	38	0.90								
FAF	0.37	0.37	0.49	0.46	0.21	78	0.40	0.40							
							0.82	0.82							
INC	0.55	0.33	0.04	0.87	0.28	46	0.70	0.45	0.88						
INF	0.38	0.41	0.63	0.44	0.27	82	0.38	0.80	0.44	0.83					
INC	0.56	0.47	0.06	0.41	0.30	37	0.30	0.36	0.44	0.35	0.93				
ITC	0.64	0.40	0.10	0.40	0.41	24	0.42	0.27	0.27	0.27	0.44	0.90			
								0.32	0.32						
KNC	0.59	0.53	0.00	0.45	0.25	59	0.34	0.47	0.47	0.48	0.65	0.41	0.88		
LEM	0.70	0.65	0.15	0.67	0.38	62	0.58	0.61	0.66	0.61	0.58		0.48	0.48	
													0.71	0.71	
													0.90	0.90	
OCR	0.81	0.41	0.10	0.59	0.45	37	0.51	0.33	0.59	0.35	0.49	0.72	0.51	0.61	0.84
POR	0.62	0.52	0.74	0.72	0.78	0.78	0.77	0.79							
RAR	0.43	0.41	0.44	0.33	0.56	0.58	0.42	0.57	0.74						

Table 3: Nomenclature of the test series

Batch	N° of specimens	Building direction	Heat treatment
E AD 0 NT	12	0°	NT
E $AD\_0°T$	12	0°	T
E $AD \sim 90°NT$	12	90°	NT
$\_AD.90°\_T$	12	90°	T
$S\_AD\_0°\_NT$	10	0°	NT
$S\_AD\_0°\_T$	8	0°	T
SAD $90°NT$	10	90°	NT
SAD 90 T	10	90°	T

3 Measurements

3.1 Roughness

Figure 4 depicts a histogram of the mean Ra values. Following fatigue testing, the fracture surfaces were examined using a Scanning Electron Microscope (SEM) to identify the cause of failure at the crack initiation point. Specifically, as Lack Of Fusions (LOFs) are commonly the most frequent and often more detrimental in terms of fatigue strength, the square root of the area (Varea) was measured, following the guidelines outlined in [10]. Measured on the surface of 5 specimens per test series along the longitudinal direction. It is evident that all test series exhibit a Ra value of approximately 0.5 μm.

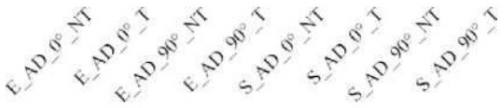

Figure 4: Ra mean value for each test series

3.2 Geometrical distortion

The geometrical distortion of each batch is expressed and measured in terms of the deflection of the specimen's axis (fa). In the earlier study [6], deflection values were utilized to assess the mean stress induced by the machine gripping system. However, in this contribution, the gross sections of specimens supplied by SISMA srl were turned to eliminate the mean stress state during fatigue testing. Consequently, the value of fa is reasonably negligible.

3.3 Hardness

Micro-hardness (HV) was measured in one specimen per test series, and the results are presented in Figure 5. Owing to the ageing hardening heat treatment, the hardness of the T series is doubled compared to the NT series. However, this phenomenon was not observed in the S batch, suggesting that the ageing treatment may not have been effective in this case.

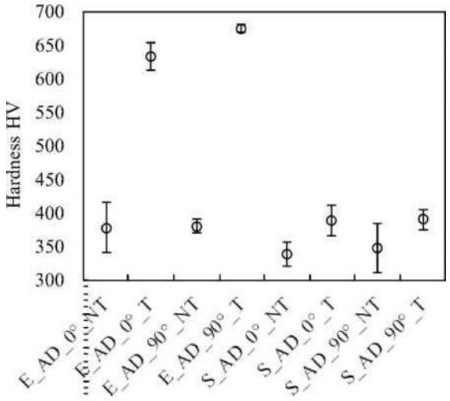

Figure 5: Microhardness (HV) results for each test series

4 Results

4.1 Fatigue test results

Figures 6(a–d) display the fatigue test results in terms of the nominal stress amplitude of the test series related to the (5) batch. The individual scatter bands correspond to the 10-90% probability of survival, derived from statistical analysis of the fatigue data.

Considering that the fatigue test results of the (E) batch were influenced by mean stresses, for comparison purposes, both the (S) batch and (E) batch results are presented in Figure 7 in terms of the SWT (Smith, Watson, and Topper)

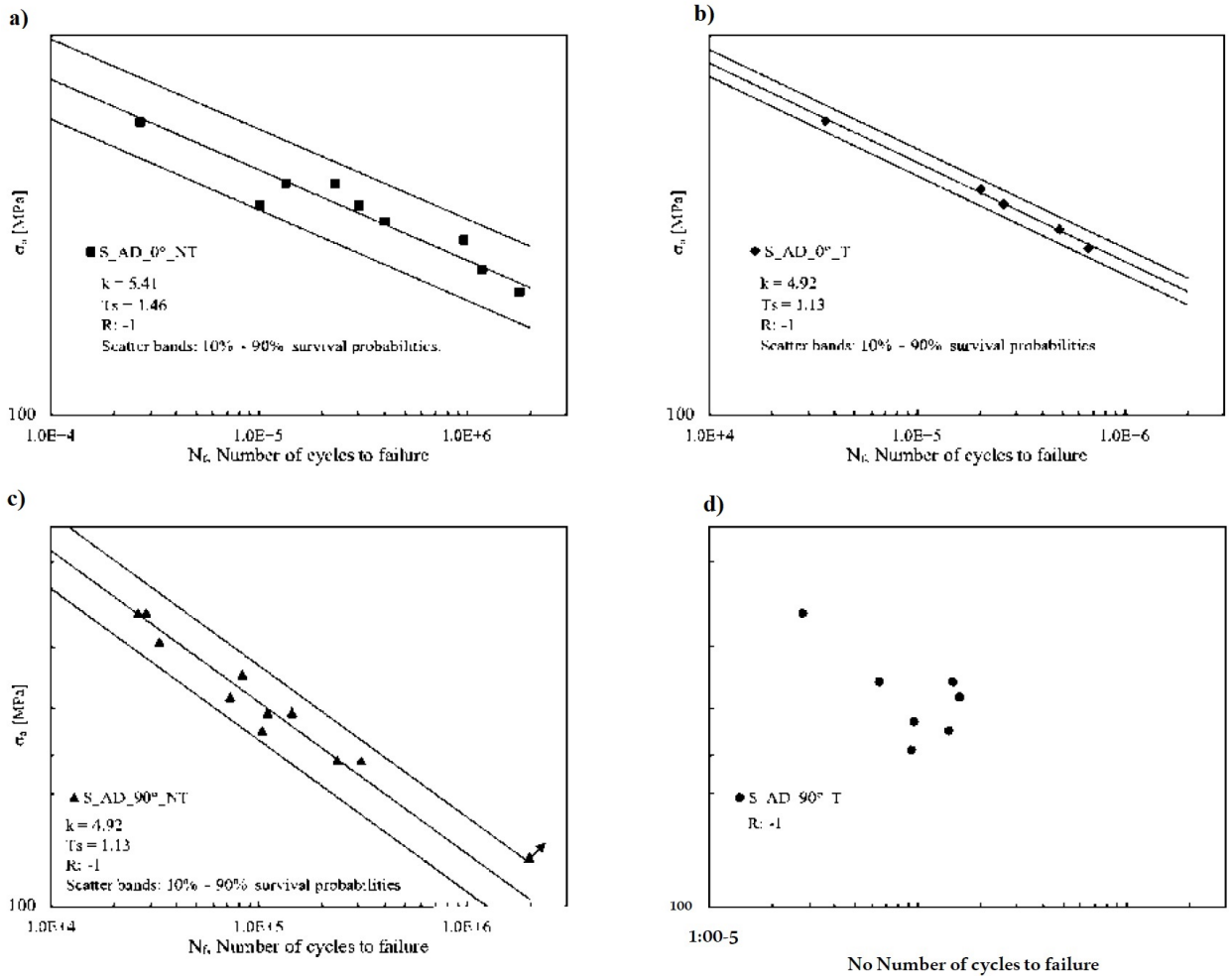

Figure 6: Fatigue test results of the test series related to the (S) batch in terms of nominal stress amplitude

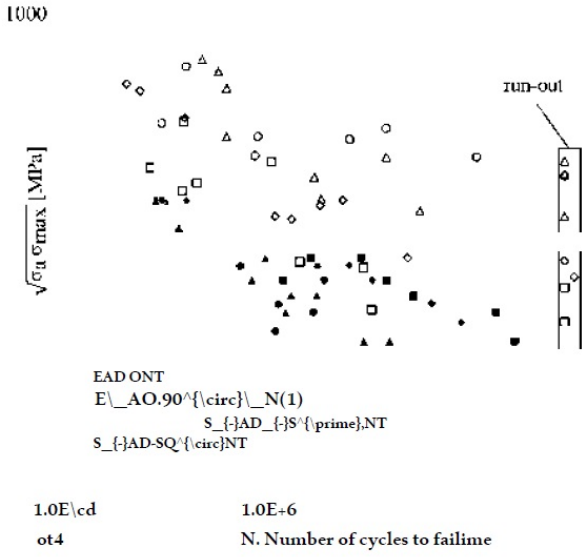

Figure 7: The constant amplitude fatigue test results of the S-batch compared to the E-batch

parameter. Due to the turning process, the SWT value of the specimens in the batch is simply the applied nominal stress amplitude.

In Fig. 7, the constant amplitude fatigue test results of the S-batch are compared to the E-batch, as previously published in [X]. The results of the S-batch are analyzed without considering mean stress effects, given the turning of the specimens' gross sections. For a comprehensive understanding of the E-batch results, readers are directed to [6].

4.2 Fractography

Figure 8 presents the fracture surfaces of specimens oriented at 0° at the crack initiation point. Consistent with recent literature, the primary cause of failure in additive manufacturing (AM) components is identified as Lack Of Fusions (LOFs), characterized by irregular shapes. As depicted in Figure 8, the effective area used to evaluate the Varea parameter is indicated by a red dotted line in each image. The selection of effective areas followed recommendations outlined [10].

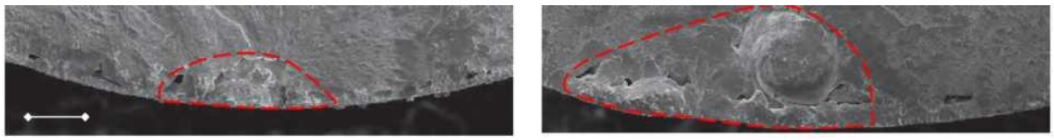

Figure 8: the fracture surfaces of specimens oriented at 0° at the crack initiation point

5 Conclusions

This study presents the experimental analysis of the defects influencing the fatigue behaviour of two batches of maraging steel specimens produced by additive manufacturing. Both batches are categorized into four test series based on build orientation and heat-treated, as-built condition, as outlined in Table 3. Similar to observations on specimens from the (E) batch, geometrical distortion caused by residual stresses was also noted in the (S) batch, particularly in specimens that were not heat-treated (NT). In contrast to the (E) batch tested in the previous work, where the effect of mean stress induced by geometrical distortion was considered, the contribution addresses this issue by turning the specimens' gross sections to prevent misalignments.

When comparing the two batches, fatigue test results were presented in terms of the SWT parameter. All fatigue data related to the (S) batch exhibited a lower fatigue strength compared to the (E) batch. Within the (S) batch's individual test series, the specimens oriented at 0°, both in (NT) and (T) conditions, showed fatigue. strength 45% to 60% higher than those oriented at 90 (evaluated at 1 million cycles). This contradicts the results of the (E) test series [6]. It's important to note that the micro-hardness values obtained on heat-treated (S) specimens are not consistent with those of the (E) batch and those reported in the literature.

The examination of fracture surfaces has revealed that fatigue failures in additive manufacturing (AM) components are primarily attributed to defects referred to in the literature as Lack Of Fusion (LOF). Consistent with existing literature, these defects exhibit irregular shapes and are predominantly situated at both the surface and the subsurface areas of the component.

In the examples depicted in Figure 8, it is evident that the effective area of defects related to the (E) batch is approximately four times smaller than those calculated for the (S) batch. Moreover, in the crack initiation area, a cluster of small defects is frequently observed. One possible interpretation is to consider such a cluster as a single defect with an effective area encompassing all the defects. However, this hypothesis has not been validated yet.

References

[1] A. Annarelli, C. Battistella, and F. Nonino, *A framework to evaluate the effects of organizational resilience on service quality*, Sustainability **12**, no. 3 (2020), 958.

[2] M.J. Donachie, *Titanium: A Technical Guide*, ASM International, 2000.

[3] J.F. Hair Jr, G.T.M. Hult, C.M. Ringle, M. Sarstedt, N.P. Danks, and S. Ray, *Partial Least Squares Structural Equation Modeling (PLS-SEM) Using R: A Workbook*, Springer Nature, 2021.

[4] R. Konečná, G. Nicoletto, L. Bubenko, and S. Fintová, *A comparative study of the fatigue behavior of two heat-treated nodular cast irons*, Eng. Fract. Mech. **108** (2013), 251–262.

[5] J.J. Lewandowski and M. Seifi, *Metal additive manufacturing: a review of mechanical properties*, Ann. Rev. Mater. Res. **46** (2016), no. 1, 151–186.

[6] G. Nicoletto, S. Maisano, M. Antolotti, and F. Dall'Aglio, *Influence of post fabrication heat treatments on the fatigue behavior of Ti-6Al-4V produced by selective laser melting*, Procedia Struct. Integrity **7** (2017), 133–140.

[7] D. Suryaningtyas, A. Sudiro, E.A. Troena, and D.W. Irawanto, *Organizational as mediating effect of organizational resilience: Culture and organizational performance*, Proc. 1st Sampoerna University-AFBE Int. Conf., SU-AFBE 2018, Jakarta, Indonesia, European Alliance for Innovation, 2019.

[8] D.D. Woods, *Four concepts for resilience and the implications for the future of resilience engineering*, Reliab. Engin. Syst. Safety **141** (2015), 5–9.

[9] W. Xu, M. Brandt, S. Sun, J. Elambasseril, Q. Liu, K. Latham, K. Xia, and M. Qian, *Additive manufacturing of strong and ductile Ti–6Al–4V by selective laser melting via in situ martensite decomposition*, Acta Mater. **85** (2015), 74–84.

[10] A. Yadollahi and N. Shamsaei, *Additive manufacturing of fatigue resistant materials: Challenges and opportunities*, Int. J. Fatigue **98** (2017), 14–31.